Proceedings of IMECE2002
ASME International Mechanical Engineering Congress & Exposition
November 17–22, 2002, New Orleans, Louisiana

IMECE2002-32098

HEAT TRANSFER IN WAVY DUCT WITH DIFFERENT CORRUGATION ANGLE

Sang Dong Hwang, Han Ho Kim and Hyung Hee Cho
Dept. of Mechanical Eng.,Yonsei University, 120-749
Seoul, Korea

Seung Bae Chen
Power systems R&D center
Samsung TECHWIN Co.LTD., Changwon, Korea

ABSTRACT

The present study investigates the effects of duct corrugation angle and flow velocity on the convective heat/mass transfer characteristics in wavy ducts applied in a primary surface heat exchanger. Local heat/mass transfer coefficients on the corrugated duct sidewall are determined using a naphthalene sublimation technique. The flow visualization technique is used to understand the overall flow structures inside the duct. The corrugation angles of the wavy ducts are 145º and 130º, and the duct aspect ratio is fixed at 7.3. The Reynolds numbers, based on the duct hydraulic diameter, vary from 1,000 to 5,000. The results show that secondary vortex flow cells, called Taylor-Görtler vortices, exist periodically in the wavy duct. Therefore, non-uniform distributions of the heat/mass transfer coefficients are obtained on the duct walls. On the pressure-side wall, high heat/mass transfer cell-shaped regions appear due to the secondary vortex flows for both corrugation angles. On the suction-side wall, the heat transfer coefficients are lower than those on the pressure-side wall. The wavy duct with the corrugation angle of 130º has the stronger strength of the secondary vortex cells resulting in higher heat/mass transfer rates on the duct wall because the sharp turn enhances the development of the secondary flow cells.

INTRODUCTION

In general, power plants and micro turbine systems, one designed to obtain high effectiveness and low pressure losses, minimum volume and weight, high reliability and low cost [1]. For gas turbine recuperators, an efficient heat exchanger is required to reduce size and increase cycle efficiency. The heat exchangers contain flow channels with various cross-sectional shapes and the channels are corrugated, curved or wavy in the main flow direction to enhance the heat/mass transfer coefficients. Several investigations have shown that the secondary flows perpendicular to the streamwise flow direction are induced by the shape of the corrugated or wavy ducts. These secondary flow motions distort the main flows and enhance the overall heat transfer coefficients. However, the friction factor increases and nonuniform heat transfer distributions are induced.

Recently, various numerical studies and approaches to the flow and heat transfer characteristics in corrugated or wavy ducts are conducted. Asako and Faghir [2] investigated the numerical studies to predict the heat transfer coefficients, friction factors, and streamlines of the corrugated duct for a laminar flow region (the Reynolds number range from 100 to 1,500). Sawyers et al. [3] investigated the steady laminar heat transfer characteristics in the corrugated channels using a combination of analytical and numerical techniques. Rokni and Sunden [4], and Rokni and Gatski [5] conducted numerical calculations of the convective heat transfer coefficients in the trapezoidal ducts. They found that enhancement of heat transfer was obtained by the change of duct shape and also pressure losses increased. Utriainen and Sunden [6] calculated the flow and heat transfer performance of a primary surface type heat exchanger and presented the Nusselt numbers and friction factors in a wavy duct. They compared the results with corresponding results of the straight ducts for various cross-sectional shapes.

Goldstein and Sparrow [7] investigated the overall heat/mass transfer characteristics for flow in a corrugated wall channel with the aspect ratio of 42.5 using a naphthalene sublimation technique. The Reynolds number varied from 500 to 3,100 in their experiments. They concluded that there exist complex secondary flows and transfer processes resulting in heat/mass transfer augmentation at the low Reynolds number. As a successive study, O'Brien and Sparrow [8] carried out heat transfer measurement to determine the convective heat transfer coefficients and measured the friction factors for the flows in a corrugated duct with the corrugation angle of 30° and aspect ratio of 10. Sparrow and Comb [9] investigated the effects of inlet conditions of a corrugated wall heat exchanger. Nishimura et al. [10] studied the detailed flow structures for various sinusoidal wavy channels using a flow visualization technique and found out the occurrence of Taylor-Görtler vortices due to the flow instabilities.

Many numerical studies have been conducted, however most of the numerical studies have not confirmed the validity of assumptions included in their calculations due to the shortage of verified experimental data. For the experimental studies, most researches deal with the flow and the average heat transfer characteristics of wavy ducts, but not with the local heat/mass transfer characteristics. Therefore, the present study focuses on the measurements of the detailed local heat/mass transfer in wavy ducts having a rectangular cross-section to apply a compact heat exchanger. For these purposes, the effects of duct corrugation angles on the heat/mass transfer are investigated. The flow patterns are examined by a flow visualization technique. Local heat/mass transfer coefficients on the corrugated wall are measured using a naphthalene sublimation technique. The Reynolds numbers, based on the duct hydraulic diameter, vary from 1,000 to 5,000. The tested corrugation angles of the wavy duct are 145° and 130° for the aspect ratio (H/W) of 7.3.

NOMENCLATURE

A : Naphthalene coated surface area
D_h : Hydraulic diameter
D_{naph} : Naphthalene vapor diffusivity in air
dy_N : Naphthalene sublimation depth
f : Friction factor in equation (5)
H : Duct height
H/W : Aspect ratio
h_m : Mass transfer coefficient
L : Duct length
$\dot{m}$: Mass transfer rate per unit area
Nu : Nusselt number
n : Exponent in equation (4)
P : Corrugation pitch
Pr : Prandtl number
Re : Reynolds number
Sc : Schmidt number
Sh : Sherwood number
$\overline{Sh}$: Average Sherwood number
U : Average duct inlet velocity
W : Duct width
x : Streamwise coordinate (Fig. 1)
y : Distance from the center in Fig. 1
z : Spanwise coordinate (Fig. 1)
$\triangle P$: Pressure drop per unit length

Greek symbols

α : Corrugation angle
ρ_{air} : Density of the air
ρ_s : Density of solid naphthalene
$\rho_{v,\infty}$: Naphthalene vapor density of the air
$\rho_{v,w}$: Naphthalene vapor density on the surface
$d\tau$: Time interval during experiment

EXPERIMENTAL APPARATUS AND PROCEDURES

Experimental apparatus

Figure 1 presents a schematic view of the experimental apparatus that consists of a blower, an orifice flowmeter, a plenum chamber and a test section. Room air entrained from the inlet contraction flows through the test duct, and is discharged out of the room by the blower (3.7 kW). The flow rates are measured using a thin plate orifice flowmeter installed between the plenum chamber and the blower. The detailed geometries and coordinate system of the test section are shown in Fig. 1(b). The corrugated duct consists of series of the pressure-side and suction-side walls, which have ten pairs. The duct has sharp-edged turns and a rectangular cross-section. Two wavy ducts which have different corrugation angles (α) of 145° and 130° are tested to investigate the effects of the corrugation angles in wavy duct. The height (H) and width (W) of the tested duct is fixed at 53.0 mm and 7.3 mm, respectively, and the length of the sidewall (L) is 33.5 mm.

Flow visualization is accomplished to understand the overall flow structures inside the wavy duct using a direct smoke injection method. The smoke tracers generated by the smoke generator are supplied to the test duct. An argon-ion laser (DANTEC, 5W) and a cylindrical lens are applied to produce a bright 2 dimensional light sheet for taking an instantaneous picture, and the path lines are captured by a digital camera (Nikon Coolpix 990). The path lines formed by the flowing smoke particles provide the information of the flow field in the wavy duct.

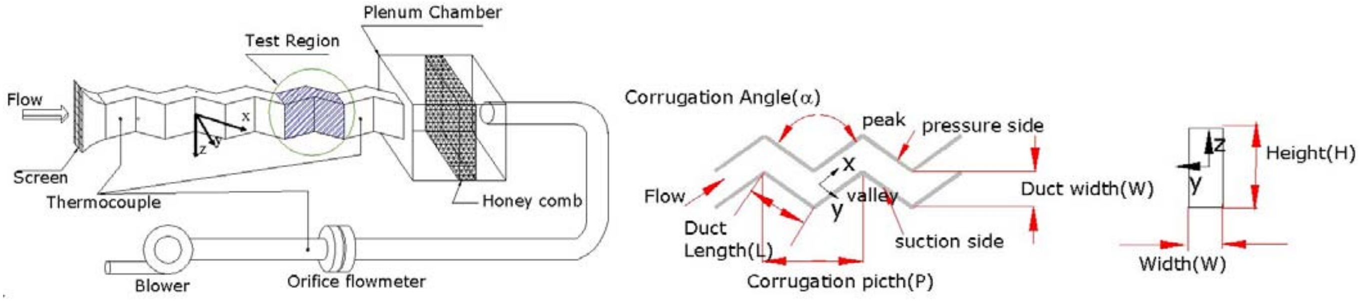

(a) Schematic diagram of experimental setup (b) Details of test section

Figure 1 Schematic view of experimental apparatus.

Mass transfer experiments are conducted using a naphthalene sublimation method instead of heat transfer experiments to obtain the detailed local transfer characteristics on the duct sidewall. The mass transfer experiments have several advantages, such as eliminating the conduction and radiation errors and obtaining the detailed local transfer coefficients. The mass transfer coefficients can be converted to the heat transfer coefficients using the heat and mass transfer analogy [11]. For the mass transfer experiments, the naphthalene coated test plates are installed at both pressure-side and suction-side walls. In order to obtain the local mass transfer coefficients, the profiles of the naphthalene coated test plates are scanned by an automated surface measuring system before and after exposure to the flow. The sublimation depths during the experiment are calculated from the differences of the surface profiles. The surface profile measuring and scanning system is consists of a LVDT (Linear Variable Differential Transformer; LB-375TA-020), a traverse system, a digital multimeter and a GPIB board. Details of the measuring system and procedures are presented by Cho and Rhee [12].

The five pressure taps having 1.0 mm in hole diameter are installed at x/(P/2)=0 on the bottom wall of the duct to measure the pressure drop through the duct. The spacing between pressure taps is the same as the corrugation pitch (P). The static pressure is measured using a digital micromanometer (FCO-510) with the accuracy of 0.001 mmH_2O.

Heat/mass transfer coefficients

The local mass transfer coefficient is defined as:

$$h_m = \frac{\dot{m}}{\rho_{v,w} - \rho_{v,\infty}} = \frac{\rho_s (dy_N / d\tau)}{\rho_{v,w}} \tag{1}$$

the naphthalene density of the inlet air is zero ($\rho_{v,\infty}$=0) in the present study, since the environmental air entrained to the test section contains no naphthalene vapor. Therefore, the mass transfer coefficient is calculated from the local sublimation depth of the naphthalene (dy_N), run time ($d\tau$), density of the solid naphthalene (ρ_s), and the naphthalene vapor density ($\rho_{v,w}$). The naphthalene vapor pressure is obtained from a correlation of Ambrose et al. [13]. Then, the naphthalene vapor density, $\rho_{v,w}$, is calculated from the perfect gas law.

The Sherwood number can be expressed as:

$$Sh = \frac{h_m D_h}{D_{naph}} \tag{2}$$

D_{naph} is based on the discussion of naphthalene properties given by Goldstein and Cho [14].

The averaged Sh is obtained by a numerical integration:

$$\overline{Sh} = \frac{\int_0^L \int_{-H/2}^{H/2} Sh\, dz dx}{A} \tag{3}$$

where A is the naphthalene coated surface area of each side wall.

The mass transfer coefficients can be converted to the heat transfer coefficients using the heat and mass transfer analogy [11].

$$\frac{Nu}{Sh} = \left(\frac{Pr}{Sc}\right)^n \tag{4}$$

The exponent n varies from 0.333 to 0.4 depending on the flow conditions.

Uncertainty of the Sherwood number using Kline and McClintock's method [15] for the single sample experiments is within 7.2% in the entire operating range of the measurements, based on a 95% confidence level. This uncertainty is attributed mainly to the uncertainty of properties of the naphthalene, such as the naphthalene saturated vapor pressure (5.1%), and diffusion coefficient of the naphthalene vapor in the air (3.0%).

Pressure drops

The friction factor, f, is defined as:

$$f = \frac{\Delta P}{4(1/D_h)(1/2)\rho_{air} U^2} = \frac{1}{2} \Delta P \frac{D_h}{\rho_{air} U^2} \tag{5}$$

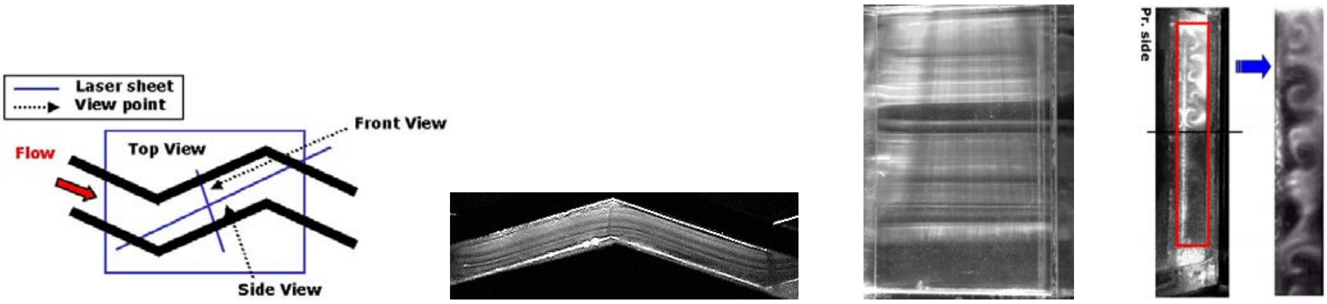

(a) View point (b) Top view (c) Side view (d) Front view

Figure 2 Smoke flow visualization results (Re=1,500).

where ΔP, ρ_{air} and U indicate the pressure drop per unit length, the density of the air and the average velocity at duct inlet, respectively. The friction factor is obtained by fitting linearly the slope of pressure drop through the wavy duct.

RESULTS AND DISCUSSION

Flow and heat transfer characteristics

There are two types of instabilities in a wavy duct at moderate flow velocity [10]. One is an instability of the separated shear layer between the main stream and a large recirculation flow (called Kelvin-Helmholtz vortex) and the other is a centrifugal instability due to the concave surface (called Taylor-Görtler vortex). The flow patterns of the smoke flow visualization are shown in Fig. 2. The photograph in the top view (Fig. 2(b)) indicates that the path lines are deflected slightly to the pressure-side wall due to the existence of corrugation angle. A small recirculation bubble is formed at the valley region of the duct. The flow separation and reattachment appear barely at the other corner (peak corner). These flow patterns appear periodically through the wavy duct. For the photograph in the side view (Fig. 2(c)), the secondary flows are observed weakly at each corner. Figure 2(d) presents the spanwise flow pattern in the front view and the secondary vortices perpendicular to the streamwise flow direction are observed. The secondary vortices (secondary flow cells) are formed due to the centrifugal instability, which caused by the shape of the corrugated duct. These vortices are considered as a kind of Taylor-Görtler vortices appeared on a concave surface.

Figure 3 shows the schematic flow patterns in the streamwise and spanwise directions based on the flow visualization results. As explained above, the streamwise flows are disturbed at the turning corner having the recirculation flow and flow separation/reattachment. The main core flow is deflected to the pressure-side wall due to the flow inertia force. The flow separation and reattachment occurs weakly at the peak corner. The secondary vortices perpendicular to the streamwise direction (Fig. 3(b)) have two vortex patterns; one is the Taylor-Görtler type secondary vortex appeared at the middle region and the other is the corner vortex affected by the end-wall. The Taylor-Görtler vortex region has several counter-rotating secondary vortex cells. The counter-rotating vortex pairs impinge on the downward flow region and are detached from the upward flow region on the pressure-side wall. On the suction-side wall, the separation/reattachment flows influence the secondary vortex flows. At the end-wall affected region, the corner vortices, which are normally observed at the corner of a non-circular duct, are formed near the top and bottom end-walls. Hence, the heat/mass transfer characteristics on the duct wall are affected strongly by these secondary vortex flow characteristics in the wavy duct.

Figure 4 presents the contour plots of the Sherwood numbers on both pressure-side and suction-side walls for the various Reynolds numbers with the corrugation angle of 145°. The “x” and “z” coordinates represent the streamwise and spanwise direction, respectively. At the Reynolds number of 1,000 (Fig.

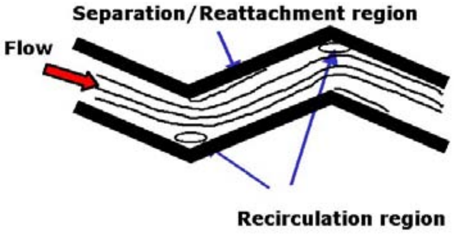

(a) Streamwise flow pattern

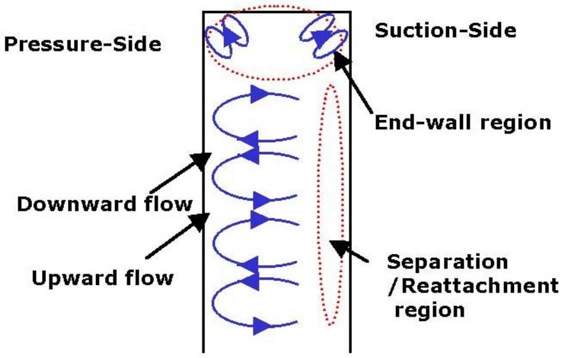

(b) Spanwise flow pattern

Figure 3 Schematic flow patterns.

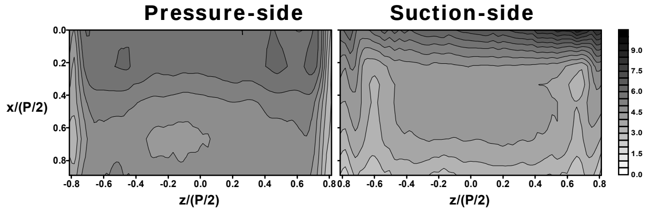

(a) Re=1,000

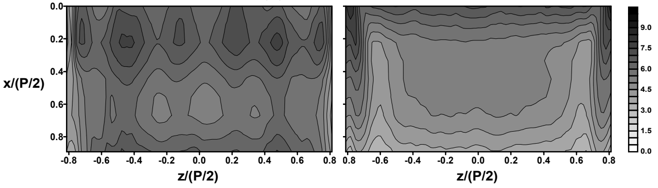

(b) Re=1,500

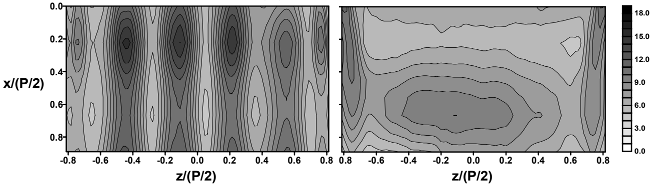

(c) Re=2,500

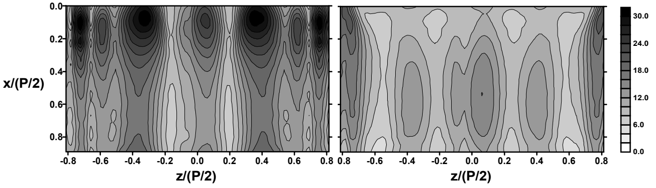

(d) Re=5,000

Figure 4 Contour plots of Sh for α =145°.

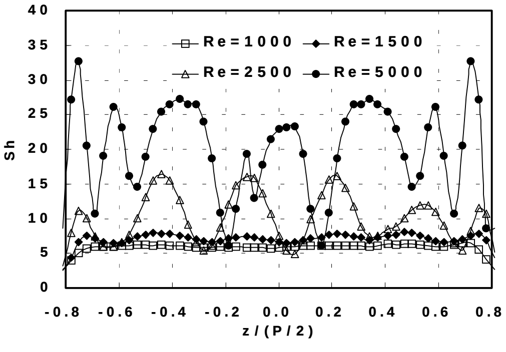

(a) Pressure-side

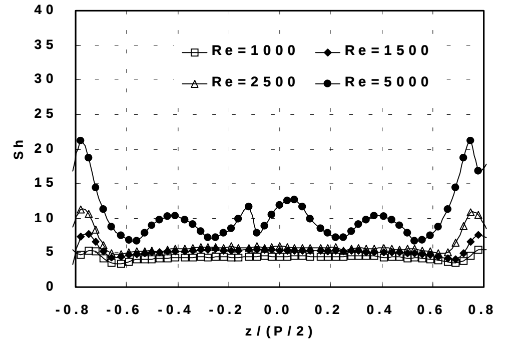

(b) Suction-side

Figure 5 Sh distributions for various Re at x/(P/2)=0.2 (α =145°).

4(a)), the Sherwood number distributions are relatively uniform along the spanwise direction, except the end-wall region (z/(P/2)≅±0.8), but the Sherwood numbers decrease along the streamwise direction on the pressure-side due to the boundary layer development of the duct flow. On the suction-side, the overall heat/mass transfer distributions indicate that the duct flow is developing along the streamwise direction. It is considered that there is no clear effect of the secondary vortex flows except the end-wall regions. For the case of Re=1,500 (Fig. 4(b)), the Sherwood numbers have peak values at z/(P/2)≅±0.5, ±0.2 and x/(P/2)≅0.2 on the pressure-side wall. These peaks are generated by the secondary vortex flows as shown in the flow visualization (Fig. 2). As explained before, the downward and upward flows are formed in the secondary vortex cells (Taylor-Görtler vortices). The downward flow on the pressure-side wall enhances the heat/mass transfer due to the impingement effects at z/(P/2)≅±0.5, ±0.2 and x/(P/2)≅0.2. On the contrary, relatively low heat/mass transfer appears at the location of z/(P/2)≅0.0, ±0.3 and x/(P/2)≅0.6 due to the upward flow. These mass transfer characteristics are observed clearly as increasing the Reynolds numbers due to enhancement of the vortex strength. On the suction-side wall, the Sherwood number distributions show the similar patterns to the case of Re=1,000, but the Sherwood number values increase due to the increased flow velocity at Re=1500. At the relatively high Reynolds of 2,500, these peak values increase on the pressure-side wall showing the clear cell traces of the secondary vortices. On the suction-side wall at Re=2,500, the high heat/mass transfer region of -0.5<z/(P/2)<0.5 and 0.4<x/(P/2)<0.7 appears due to the reattachment of separated flow at the edge of duct turning. At the highest Reynolds number (Re=5,000) in the present study, relatively high heat/mass transfer cell regions are also observed on the suction-side wall, but those regions do not appear at the lower Reynolds numbers. The reason is that the intensity and size of the secondary Taylor-Görtler vortices increase with increasing the flow velocity resulting in influencing on the suction-side wall.

Figure 5 shows the comparisons of the Sherwood number distributions for the various Reynolds numbers on each pressure-side and suction-side wall at x/(P/2)=0.2. On the pressure-side wall (Fig. 5(a)), the Sherwood numbers at Re=1,000 are uniform along the spanwise direction, except the end-wall region. As the Reynolds number increases to Re=2,500, the local peaks in the Sherwood number appear clearly at z/(P/2)≅±0.5, ±0.2 due to the secondary vortex flows. On the suction-side wall, the Sherwood number distributions are uniform along the spanwise direction for Re=2,500. However, the local peaks in the Sherwood number appear at

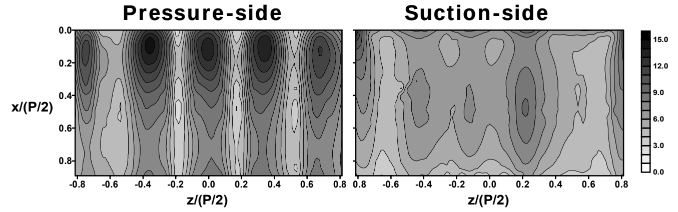

(a) Re=1,500

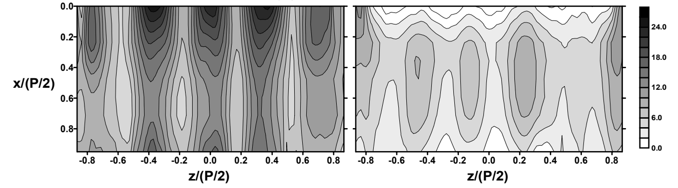

(b) Re=2,500

Figure 6 Contour plots of Sh for α =130º.

Re=5,000 due to the increased intensity and size of the secondary Taylor-Görtler vortices. At both end-wall regions, the Sherwood number has the local peaks at z/(P/2)≅±0.75 due to the secondary corner vortices induced by the existence of the end-wall.

Effects of the corrugation angle

Figure 6 presents the contour plots of the Sherwood numbers on the pressure-side and suction-side walls for the corrugation angle of 130º. When the corrugation angle decreases to 130º, the contour plots indicate more clear cell traces and higher peak values than those of the corrugation angle of 145º at the same Reynolds number. It is considered that the wavy duct of the corrugation angle of 130º has more sharp turns and curvatures to the streamwise direction than that of the corrugation angle of 145º resulting in generation of larger centrifugal force. Therefore, the strength of the secondary vortex cells increases and the enhancement of the heat/mass transfer increases. On the suction-side walls, traces of the vortex cells appear at the lower Reynolds number of 1,500 instead of the Reynolds number of 5,000 in case of the corrugation angle of 145º. These vortex cells are more clearly observed and enhance the Sherwood number. It is because the intensity and the size of the secondary Taylor-Görtler vortices increase as the corrugation angle decreases.

Figure 7 presents the comparison of the Sherwood numbers for the different corrugation angles of 145º and 130º at x/(P/2)=0.2. On the pressure-side wall, the peak values of the Sherwood number increase with decreasing the corrugation angles due to the increased intensity of the secondary vortices at the same Reynolds number. At Re=2,500, the local peaks of the Sherwood number exist at z/(P/2)≅±0.5 and ±0.2 for the corrugation angle of 145º except near the end-wall regions. However, the local peaks exist at z/(P/2)≅0.0 and ±0.3 for the corrugation angle of 130º. The reason is that the size and strength of the secondary Taylor-Görtler vortices increase as the corrugation angle decreases due to the stronger curvature effects, resulting in the number of vortex cells decrease. On the suction-side wall, the uniform Sherwood number distributions are obtained for the corrugation angle of 145º except the end-wall regions (z/(P/2)≅±0.8). However, for the corrugation angle of 130º, the local peaks appear weakly at z/(P/2)≅±0.2, ±0.5 due to the secondary vortex flows.

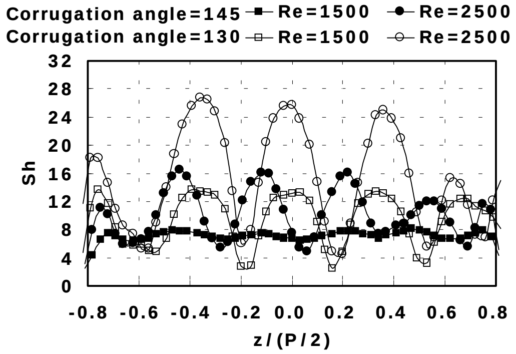

(a) Pressure-side

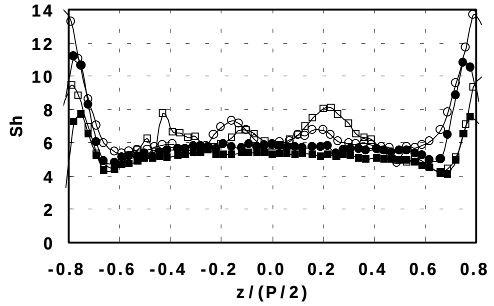

(b) Suction-side

Figure 7 Comparison of Sh for different corrugation angle at x/(P/2)=0.2.

The average Sherwood numbers are shown in Fig. 8. On the pressure-side wall, the average Sherwood number increases linearly with increasing the Reynolds number as expected. The higher average Sherwood number is obtained with the smaller corrugation angle of 130º due to the increased secondary vortices at the same Reynolds number. On the suction-side wall, the average Sherwood numbers are lower than those on the pressure-side wall. It is considered that the effects of the secondary rotating vortices on the suction-side wall are much weaker than those on the pressure-side wall. For the corrugation angle of 130º, the average Sherwood numbers increase slightly from those of the corrugation angle of 145º due to the effects of the secondary vortices.

Figure 9 presents the friction factors with increasing Reynolds number for the different corrugation angles. The friction factor in the wavy ducts decreases with increasing Reynolds number in both corrugation angles. The fiction factors with the corrugation angle of 130º are about one and half times greater than those with the corrugation angle of 145º. The

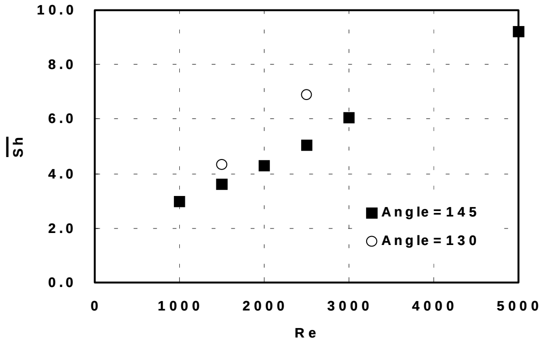

(a) Pressure side

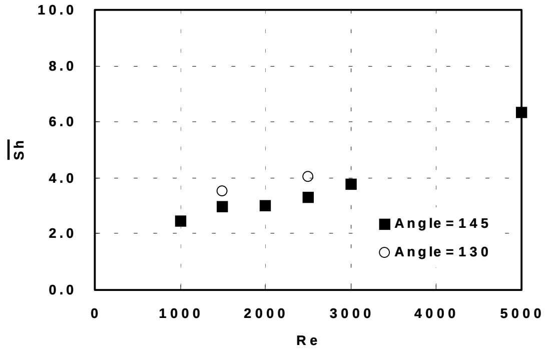

(b) Suction-side

Figure 8 Average Sh distributions with increasing Re.

reason is that the stronger secondary vortices with the smaller corrugation angle disturb more vigorously the main flow resulting in increasing pressure loss.

CONCLUSION

The present study investigates the convective heat/mass transfer characteristics in wavy ducts of a primary surface heat exchanger. The effects of the corrugation angle of the wavy duct on the heat/mass transfer are investigated. The flow visualization indicates that secondary vortices perpendicular to the streamwise direction are generated due to the wavy duct curvature, and the duct secondary flow is classified into two regions, such as the Taylor-Görtler vortex flow region and the corner vortex region affected by the end-wall.

Non-uniform heat/mass transfer coefficients are obtained on the duct wall due to the secondary Taylor-Görtler vortices and the end-wall corner vortices. On the pressure-side wall, the secondary Taylor-Görtler vortices enhance the heat/mass transfer significantly. However, the heat/mass transfer is low on the suction-side due to the boundary layer type flow with the flow separation and reattachment at the low Reynolds number except the end-wall region. However, the effects of the secondary vortices appear on the suction-side wall at the high Reynolds number.

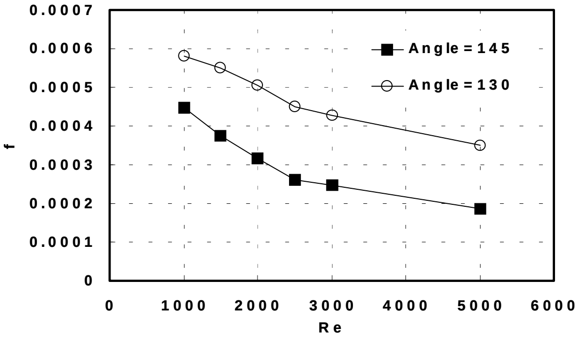

Figure 9 Friction factor distributions with increasing Re.

For the smaller corrugation angle of 130°, the intensity and size of the secondary vortex flows increase due to the strong curvature effects, thus the higher heat/mass transfer rates are obtained than those of the corrugation angle of 145°. The effects of the secondary vortex cells appear on the suction-side wall at the relatively lower Reynolds of 1,500 with the smaller corrugation angle of 130°.

The average Sherwood number on pressure-side wall is higher than that on the suction-side wall due to the effects of the secondary vortices. The average Sherwood numbers increase with decreasing the duct corrugation angle due to the enhanced strength of the secondary Taylor-Görtler vortices at the same Reynolds number. More pumping power (pressure loss) is required with the smaller corrugation angle of 130° than that with the corrugation angle of 145° due to the stronger secondary vortex flows.

ACKNOWLEDGMENTS

This work was supported by the National Research Laboratory program of KISTEP (Korea Institute of Science and Samsung TECHWIN Co. LTD.

REFERENCES

1. McDonald, C. F. and Wilson, D. G., 1996, "The Utilization of Recuperated and Regenerated Engine Cycles for High-efficiency Gas Turbines in the 21st Century," Applied Thermal Eng. **16(8)**, pp. 635-653.
2. Asako, Y. and Faghri, M., 1987, "Finite-Volume Solutions for Laminar Flow and Heat Transfer in a Corrugated Duct," J. Heat Transfer, **109**, pp. 627-634.
3. Sawyers, D. R., Sen, M. and Chang, H. C., 1998, "Heat Transfer Enhancement in Three-dimensional Corrugated Channel Flow," Int. J. Heat and Mass Transfer, **41**, pp. 3359-3573.

4. Rokni, M. and Sunden, B., 1998, "3D numerical investigation of turbulent forced convection in wavy ducts with trapezoidal cross-section," Int. J. Numerical Methods for Heat & Fluid Flow, **8**, pp. 118-141.
5. Rokni, M. and Gatski, T. B., 2001, "Predicting Turbulent Convective Heat Transfer in Fully Developed Duct Flows," Int. J. Heat & Fluid Flow, **22**, pp. 381-392.
6. Utriainen, E. and Sunden, B., 2000, "Numerical Analysis of a Primary Surface Trapezoidal Cross Wavy Duct," Int. J. Numerical Methods for Heat & Fluid Flow, **6**, pp. 634-648.
7. Goldstein, L. Jr. and Sparrow, E. M., 1977, "Heat/Mass Transfer Characteristics for Flow in a Corrugated Wall Channel," J. Heat Transfer, **99**, pp. 187-195.
8. O'Brien, J. E. and Sparrow, E. M., 1982, "Corrugated-Duct Heat Transfer, Pressure Drop, and Flow Visualization," J. Heat Transfer, **104**, pp. 410-416.
9. Sparrow, E. M. and Comb, J. W., 1983, "Effect of Interwall Spacing and Fluid Flow Inlet Conditions On A Corrugated-wall Heat Exchanger," Int. J. Heat/Mass Transfer, **26(7)**, pp. 993-1005.
10. Nishimura, T., Yano, K., Yoshino, T. and Kawamura, Y., 1990, "Occurrence and Structure of Taylor-Görtler Vortices Induced in Two-Dimensional Wavy Channels for Steady Flow," J Chemical Engineering of Japan, **23**, pp. 697-703.
11. Eckert, E. R. G., 1976, Analogies to Heat Transfer Processes, in Measurements in Heat Transfer, ed. Eckert, E. R. G. and Goldstein, R. J., pp. 397-423, Hemisphere Pub., New York.
12. Cho, H. H. and Rhee, D. H., 2001, "Local Heat/Mass Transfer Measurement on the Effusion Plate in Impingement/Effusion Cooling System," J. Turbomachinery, **123**, pp. 601-608.
13. Ambrose, D., Lawrenson, I. J. and Sparke, C. H. S., 1975, "The Vapor Pressure of Naphthalene," J. Chemical Thermodynamics, **7**, pp. 1173-1176.
14. Goldstein, R. J. and Cho, H. H., 1995, "A Review of Mass Transfer Measurements Using Naphthalene Sublimation, Experimental Thermal and Fluid Science," **10**, pp. 416-434.
15. Kline, S. J. and McClinetock, F., 1953, "Describing Uncertainty in Single Sample Experiments," Mech. Engineering, **75**, pp. 3-8.